Letter

Ultrafast charge transfer dynamics at the MoS_2/Au interface observed via optical spectroscopy under ambient conditions

Tao Yang [1,*] Zhipeng Huang [1] Stephan Sleziona [1] Eckart Hasselbrink [2] Peter Kratzer [1]
Marika Schleberger [1] R. Kramer Campen [1] and Yujin Tong [1,†]
[1]*Faculty of Physics, University of Duisburg-Essen, 47057 Duisburg, Germany*
[2]*Faculty of Chemistry, University of Duisburg-Essen, 45117 Essen, Germany*

(Received 15 January 2025; revised 23 June 2026; accepted 29 June 2026; published 27 July 2026)

Integrating atomically thin transition metal dichalcogenides (TMDCs) with metallic surfaces is an effective strategy to leverage their exceptional properties in advanced devices and catalysts, as it promotes efficient charge carrier injection and extraction from TMDC monolayers. Light-matter interactions in TMDC monolayers predominantly occur at the *K* point, making the charge carrier dynamics at this point essential for optimizing charge transfer efficiency. However, direct probing of the dynamics at the *K* point of TMDCs interfaced with metal substrates remains challenging. In this Letter, we employed pump-probe azimuth- and polarization-dependent final-state sum frequency generation spectroscopy to investigate the ultrafast dynamics of charge transfer at the *K* point of a MoS_2 monolayer on an Au substrate. We observed ultrafast injection of photoexcited hot electrons from Au into the monolayer MoS_2 conduction band minimum, followed by a fast return (∼2 ps) and a trap-state-mediated slow return (∼60 ps) processes, driven by an internal electric field. The direct optical observation of the full electron dynamics at the *K* point of MoS_2 monolayer in ambient conditions provides valuable insights into optimizing the transfer of charge carrier across the TMDC/metal interface through optimized contacts, informing the design of advanced TMDC-based devices with enhanced charge transfer rates.

DOI: 10.1103/t3fz-gqf9

Introduction. Transition metal dichalcogenide (TMDC) monolayer/metal heterojunctions are widely used to exploit the distinctive electronic and optical properties of TMDCs in optoelectronics and photocatalysis [1–4]. Metals in these configurations conventionally act as integral components within electrical circuits and/or function as electron collectors. However, compared to conventional metal/semiconductor junctions found in silicon-based electronics, employing a metal/TMDC junction in a device confronts several unresolved challenges. Foremost among these challenges are high contact resistance (around 1 kΩ μm (the convention for using this unit in two-dimensional systems is delineated in Refs. [5,6]), which is more than ten times that of silicon-based devices) [7–9] and an unknown charge transfer rate [10], impeding the development of devices characterized by low power consumption and superior performance.

The high electrical contact resistance arises predominantly from the Schottky barrier, which results from the difference between the work function of the metal and the electron affinity of the semiconductor, as well as metal-induced gap states [9,11]. Efforts to address this involve minimizing the Schottky barrier width by doping [7,12] or suppressing gap states to attain an Ohmic contact [9]. The charge transfer rate is pivotal in determining the maximum rate at which a device can inject or extract charge carriers from TMDC monolayers and thus holds particular significance in applications such as field-effect transistors and photodetectors.

Studies on ultrafast charge carrier dynamics within TMDC monolayers have primarily focused on exciton-related dynamics, encompassing processes such as the formation and recombination of excitons [13–20] and trions [21]. However, efficient device operation depends on the dissociation of excitons into free charge carriers and their subsequent transfer across interfaces. Given the prevalence of the metal/semiconductor junction in TMDC-based devices, understanding the dynamics of free charge carriers across this interface is critical. Earlier investigations of hot-carrier dynamics at TMDC/metal interfaces often involve plasmonic nanostructures [22–24], which may not fully capture real-world device conditions with standard metal contacts.

Ultrahigh vacuum (UHV)-based time-resolved photoemission is a powerful tool to study hot-carrier dynamics at well-ordered TMDC/metal interfaces, ideally single-crystal monolayers on extended metal substrates [7,10,25,26]. For example, time-resolved photoemission electron microscopy (tr-PEEM) revealed ultrafast hot-electron transfer across a metal-semiconductor interface [10], but its momentum window is restricted near the Γ point and cannot directly probe dynamics at the *K* point. Time- and angle-resolved photoemission spectroscopy (tr-ARPES) can access the *K* point and resolve momentum-dependent relaxation [18,25], yet photoemission generally requires UHV and exposed, unencapsulated surfaces.

*Contact author: tao.yang@uni-due.de
†Contact author: yujin.tong@uni-due.de

Pump-probe optics is widely used to probe carrier and exciton dynamics in TMDCs across diverse environments [3,27–29]. Yet in TMDC/metal heterostructures, the metal background can dominate and obscure the TMDC dynamics. This limitation can be mitigated with second-order nonlinear optics using azimuthal- and polarization-resolved detection. In our previous work [30,31], the distinct structural symmetries of the TMDC and metal enable selective isolation of the monolayer signal via appropriate polarization combinations. Hong *et al*. recently conducted a study on the transfer of hot charge carriers between bulk MoS_2 and three distinct Au surfaces [32]. The nature of bulk MoS_2, in conjunction with the over-band-gap pump excitation, poses a significant challenge in tracking the dynamics at the *K* point. While nonlinear probes are not intrinsically momentum resolved, practical valley selectivity can be achieved by choosing probe photon energies guided by the band structure: for monolayer TMDCs, direct-gap light-matter interactions are concentrated at the *K* point [3,27,28]. Thus, pump-probe second-order nonlinear optics provides an all-optical route to charge transfer dynamics at the *K* point in TMDC/metal, including potentially buried interfaces, under ambient conditions.

In this Letter, we employ pump-probe final-state sum frequency generation (FS-SFG) spectroscopy (based on second-order nonlinear optical process) with azimuthal- and polarization-dependent detection to selectively probe femtosecond-resolved charge transfer dynamics at the *K* point in the MoS_2/Au heterostructure under ambient conditions. We have previously demonstrated that the A and B excitons of MoS_2 monolayers are quenched when it is in contact with the Au substrate. This suggests that the response is dominated by free charge carriers due to pronounced dielectric screening and substrate-induced doping effects [31]. Building on this, we resolve free-carrier dynamics without significant excitonic contributions. Using a pump photon energy below the MoS_2 band gap, we reveal the ultrafast transfer of hot electrons from the Au substrate across the heterojunction and their subsequent relaxation toward the conduction band minimum (CBM) at the *K* point in the MoS_2 monolayer.

Results and discussion. The charge carrier dynamics of MoS_2/Au were explored by pump-probe SFG spectroscopy using the setup illustrated in Fig. 1(a). The sum of the photon energies of the narrowband visible beam (1.56 eV) and the photon energy of the broadband IR beam, which was tuned from 0.28 to 0.41 eV, covered an energy window around the band gap at the *K* point. When this sum is resonant with an allowed transition, the SFG signal is enlarged. The central photon energy of the ultrashort pump beam (45 fs) was 1.56 eV, which is lower than the band gap of monolayer MoS_2 on Au (1.65 eV) [31]. The polarization of each probing beam can be set to either *p* (parallel) or *s* (perpendicular) relative to the plane of incidence. For example, consider the *spp* polarization combination, which indicates an *s*-polarized SFG, a *p*-polarized visible beam, and a *p*-polarized infrared beam. All experiments were conducted under ambient conditions at ∼21.5 °C. Further details about sample preparation and characterization (including optical microscopy and atomic force microscopy images), laser setup, characterization of the ultrashort laser pulses, and data analysis can be found in the Supplemental Material [33]. The

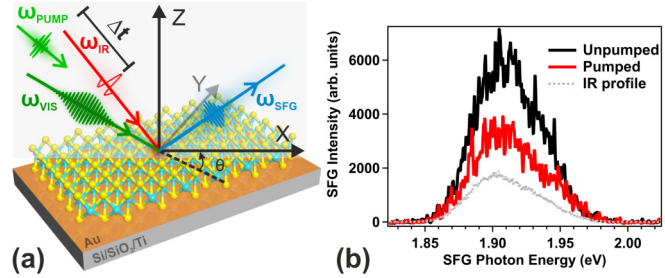

FIG. 1. Azimuth-dependent SFG intensity (i.e., intensity is a function of azimuthal angle) and dynamics for MoS_2 monolayer on Au. (a) Schematic representations of an exfoliated MoS_2 monolayer on Au substrate investigated by the time- and polarization-resolved FS-SFG. (b) The FS-SFG raw spectra collected before and after the arrival of the pump under *spp* polarization combination. The gray curve represents the spectral profile of IR collected on the Au substrate, which is plotted against the SFG photon energy.

Raman and photoluminescence spectra of the same sample have been published in our previous work [31].

Figure 1(b) shows FS-SFG spectra of MoS_2/Au recorded in *spp* before and after pump arrival; sub-band-gap pumping produces a pronounced bleaching near time zero. To interpret this response, we analyze both its azimuthal and temporal dependences. Figures 2(a) and 2(b) show the azimuth-dependent SFG intensity of bare (polycrystalline) Au and MoS_2/Au, respectively, serving as a guide for spectral acquisition under different polarization combinations. Unlike the isotropic response of the Au substrate, the FS-SFG intensity of MoS_2 monolayer on Au exhibits a sixfold symmetry, which is consistent with literature reports [34–37] and our previous studies [30,31]. These distinct patterns reflect the different symmetries: 2H-MoS_2 belongs to the D_{3h} point group [34–36], whereas the (polycrystalline) metal substrate is effectively $C_{\infty v}$ with respect to the surface normal. This symmetry contrast enables selective probing of the monolayer or substrate $\chi^{(2)}$ response by choosing appropriate polarization combinations. A full derivation based on group theory and the complete experimental data set have been reported in our previous study [30]. One key conclusion of those works is that a sixfold azimuthal intensity pattern indicates a signal originating exclusively from the MoS_2 monolayer; otherwise, the pattern becomes threefold (Fig. S4(a) in the Supplemental Material [33]). In the latter case, the dynamics is much more complicated (Figs. S4(b) and S5 in the Supplemental Material [33]). Here, we focus on charge transfer into and out of the TMDC and therefore analyze the *spp* data in detail. For the following experiment, data on the dynamics of MoS_2/Au were collected at one of the six azimuthal angles where the FS-SFG intensity reaches a maximum. In contrast, the dynamics of bare Au was studied at one of arbitrarily chosen azimuthal angles under *ppp* polarization combination [Fig. 2(a)]. The transient FS-SFG signal of bare Au and MoS_2/Au are shown in Fig. 2(c). All signals have been normalized to those at the negative delay. The *y* axis represents the square root of the normalized SFG intensities.

The dynamics of MoS_2 monolayer on Au shows a dramatic difference compared to that observed for bare Au at the same pump fluence, as illustrated in Fig. 2(c). The extent

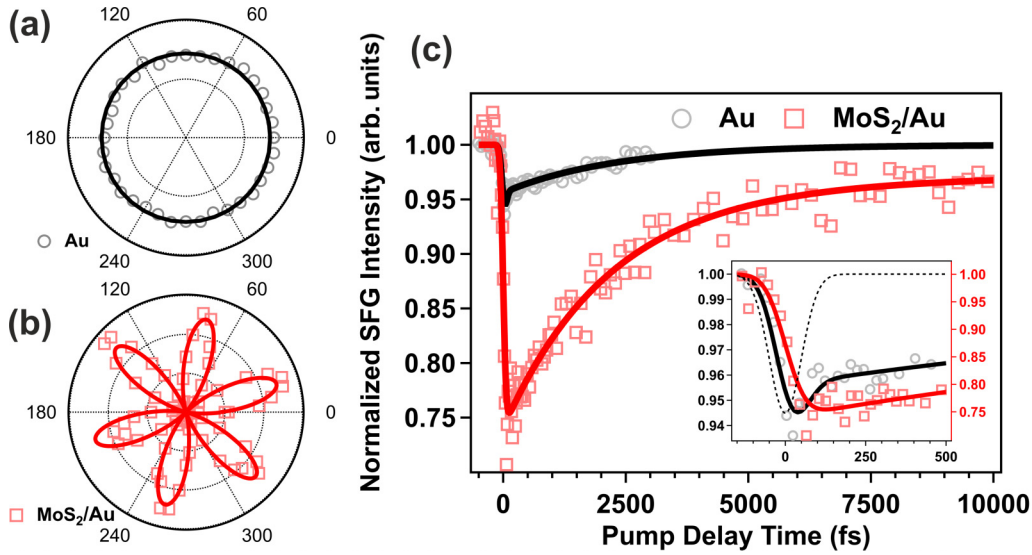

FIG. 2. Azimuth-dependent FS-SFG intensity and ultrafast dynamics of the bare Au substrate and the MoS_2 monolayer on Au. (a) Azimuth-dependent FS-SFG intensity of bare Au under *ppp* polarization combination. (b) Azimuth-dependent FS-SFG intensity of MoS_2/Au under *spp* polarization. (c) Transient signal changes were observed for bare Au and MoS_2/Au with pumping. The gray circle (black solid line) and red square (red solid line) represent the raw data (fitted curve) of bare Au and MoS_2/Au under *ppp* and *spp* polarization combinations, respectively. The inset shows the short-term behavior of both samples around SFG signal bleaching maximum with different *y*-axis scales. The black dashed line in the inset depicts the simulated instrument response.

of maximum bleaching differs significantly: Bare Au exhibits a bleaching of around 7%, while the FS-SFG signal for MoS_2/Au shows a much larger bleaching of approximately 30%. Following the maximum bleaching, the signal from bare Au undergoes an ultrafast recovery process within 100 fs, which is absent in the case of MoS_2/Au. After 3 ps, the SFG signal from bare Au recovered to 99% of its initial value, whereas the recovery for MoS_2/Au remains at about 92%. Even at a delay of 100 ps, the SFG signal of MoS_2/Au has not fully recovered to its initial state (see Fig. S6 for longer dynamics in the Supplemental Material [33]).

To model the observed dynamics, a biexponential function convoluted with a Gaussian function was applied to fit the data for both bare Au and MoS_2/Au. The width of the Gaussian function (σ) was determined to be 54 fs, based on the pump-IR cross-correlation trace on Au. A detailed explanation of the procedure can be found in the Supplemental Material [33]. For Au, two time constants were extracted with values of $\tau_1 = 10 \pm 0.1$ fs and $\tau_2 = 2.31 \pm 0.20$ ps. These values correspond to the well-understood two relaxation processes of hot electrons in metals: electron-electron scattering and electron-phonon scattering [38–40]. For the MoS_2/Au system, two time constants were extracted: $\tau_1 = 2.19 \pm 0.17$ ps, and $\tau_2 = 59 \pm 25$ ps. These time constants describe the recovery process following maximum bleaching.

Since the pump photon energy is smaller than the band gap of MoS_2 monolayer on Au, direct excitation of MoS_2 is impossible. However, hot electrons can be excited in the Au film of the heterostructure. The probe (SFG) photon energy matches the band gap of the MoS_2 monolayer at the *K* point in momentum space. Therefore, the observed bleaching and recovery of the FS-SFG signal from MoS_2 after pumping must be attributed to the dynamics at the *K* point. This bleaching in MoS_2 can be attributed exclusively to the occupation of CBM states by these transferred hot electrons, which leads to a band filling or Pauli blocking effect [41–43].

Turning our attention to the recovery of the FS-SFG signal, the bleaching arises from band filling or Pauli blocking, while its recovery indicates the release of transiently occupied CBM states as the hot electrons leave. This raises an important question: Where do these hot electrons go? Given that no holes are generated in MoS_2 during the sub-band-gap pumping, recombination with holes in MoS_2 can be ruled out. Instead, the hot electrons transferred from Au to MoS_2 create a charge imbalance at the interface, generating an interfacial electric field. This field drives the transfer of electrons back to Au, restoring charge neutrality [24].

It is worth noting that there can be a difference in charge transfer rates between the forward (from Au to MoS_2) and backward transfer. The forward transfer, mostly driven by hot electrons in Au, is relatively fast because these hot electrons possess sufficient energy to overcome the Schottky barrier at the interface. Studies estimate this barrier for MoS_2 monolayer on Au to be approximately 0.5–1.0 eV [44–46]. With a pump photon energy of 1.56 eV, the photoexcited hot electrons in Au easily overcome this barrier. In contrast, the backward transfer occurs through transfer of electrons close to the Fermi level, leading to a somewhat slower transfer rate. Interestingly, the first time constant of 2.19 ps observed for MoS_2/Au aligns closely with the 2.31 ps required for hot electrons in Au to reach equilibrium with the phonons. This correlation suggests that the 2.19 ps reflects the equilibration of CBM occupation in MoS_2 with the overall Fermi level of the MoS_2/Au system and the process by which hot electrons in MoS_2 are returned to Au. A prior tr-PEEM study reported a shorter ~400 fs time constant for hot-electron transfer back to Au [10]. However, their probe window was constrained to the vicinity of the Γ point of MoS_2, making their measurement

specific to electron dynamics near that region of momentum space. In contrast, our experiment directly captures ultrafast hot-electron dynamics at the CBM at the K point. Notably, the dynamics at K point can differ significantly if the MoS_2 monolayer is placed on a dielectric substrate, such as SiO_2, as illustrated in Fig. S8 in the Supplemental Material [33]. The presence of excitons in such cases complicates the dynamics compared to the free charge carrier dynamics focused in this study.

To corroborate the aforementioned interpretation of the 2.19 ps observed for MoS_2/Au, the charge transfer between Au and MoS_2 was analyzed using a simple kinetic model. In brief, the proposed kinetic model posits that the transient SFG response in bare Au is proportional to the electron temperature following pump excitation, with the maximum temperature of the electrons calculated via the two-temperature model [39,47]. For the MoS_2/Au system, the transient FS-SFG response is determined by the CBM occupation in MoS_2. To describe the occupation of the CBM in $MoS_2[n(t)]$, it is necessary to consider the transfer of electrons from Au to MoS_2 and the back-transfer process. The nonequilibrium population of the MoS_2 orbitals near the CBM follows a first-order differential equation, which is solved to give the occupation of the CBM of the MoS_2 monolayer. The unoccupied population $[1 - n(t)]$ at the CBM of MoS_2 is illustrated in Fig. S9 in the Supplemental Material [33]. A fit to the trace suggests a decay time constant of 2.31 ps, matching the $\tau_2 = 2.31$ ps observed for the bare Au. Further details can be found in the Supplemental Material's kinetic model section [33].

Regarding the slowest recovery process (59 ps) observed for MoS_2 on Au, further evidence from the time-dependent changes in the spectral centroid will facilitate a deeper understanding. The spectral centroid, defined as the center of mass of a spectrum, was analyzed as a function of pump-probe delay as it is expected to reflect the real-time occupation dynamics of CBM states in the MoS_2 monolayer. Occupation of CBM states reduces the strength of low-energy transitions in comparison to high-energy transitions, leading to a blueshift in the spectral centroid. As shown in Fig. S10 of the Supplemental Material [33], MoS_2/Au exhibits a pump-induced blueshift that disappears over time. This blueshift results from the gradual occupation of CBM states by hot electrons injected from the Au substrate. The subsequent transfer of hot electrons facilitates low-energy photoexcitation, observed as a decay of the blueshift. A single exponential fit gives a decay time constant of 2.37 ± 0.76 ps, matching the time for hot electrons to leave the CBM. While this suggests the complete release of the CBM states and full recovery of the FS-SFG signal within ~2 ps, only partial recovery is observed, indicating persistent screening effects even after electron extraction from the CBM of MoS_2. The additional long-lived screening effect may arise from a defect-mediated trap state situated close to the CBM [29,48–51]. These defects, such as S vacancies observed before via scanning tunneling spectroscopy [50] and tr-APRES [51], can trap a portion of the hot electrons transferred from Au. This trapping results in prolonged weak bleaching of the FS-SFG signal due to Coulomb repulsion between trapped and excited electrons during probing. Ultimately, the trapped hot electrons return to the Au substrate, resulting in full recovery of the FS-SFG signal.

Based on the above analysis, we summarize the observed dynamics in Fig. 3. At negative delay, the FS-SFG signal originates primarily from the MoS_2 monolayer ensured by choosing an appropriate polarization combination. Upon the arrival of the pump pulse, hot electrons are excited instantaneously in the Au substrate, while the MoS_2 remains unaffected due to the sub-band-gap photon energy. On an ultrashort timescale, a significant number of hot electrons transfer from Au to the CBM of MoS_2, also populating trap states at the K point (process 0 in Fig. 3). Subsequently, a charge redistribution-induced internal electric field drives the return of equilibrated electrons from the CBM of MoS_2 to Au (process 1 in Fig. 3). Thereafter, the small amount of hot electrons trapped in the defect state gradually return to Au at a much slower rate, contributing to the second recovery process (process 2 in Fig. 3). The present study provides direct observation of the injection and extraction of hot electrons at the CBM located at the K point of the MoS_2. The extracted time constants provide compelling evidence of the underlying mechanisms governing the charge transfer and relaxation processes.

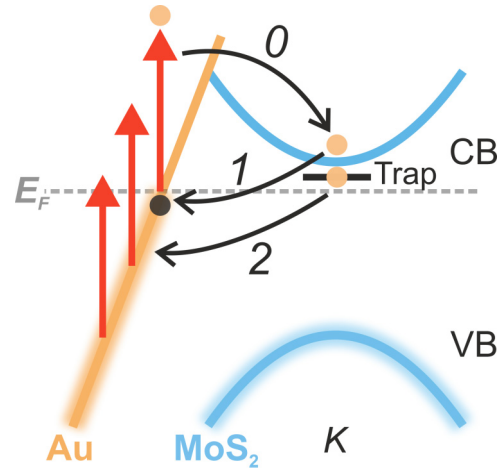

FIG. 3. Charge transfer process within the MoS_2/Au heterostructure, illustrated in a simplified partial band-structure picture of Au and MoS_2 monolayer around the K point in momentum space. The detailed band structure for both Au and MoS_2 monolayer around the K point can be found in Fig. S11 in the Supplemental Material and in Refs. [24,52]. The slanted orange line in the figure stands for the edge of the continuum of metal bulk states near K point. The blue parabolas represent the CBM and VBM of the MoS_2 monolayer. The short black line situated below the CBM denotes the trap (defect) state. The blurred curves show that states below the Fermi level are occupied. The red arrows symbolize the photoexcitation process on Au by the pump pulse. The numbered black arrows, labeled 0, 1, and 2, respectively, represent the following processes: the transfer of hot electrons from the Au to the CBM and trap state of MoS_2, the return of equilibrated electrons to Au from the CBM, and the relaxation of trapped electrons back to Au.

Conclusion. In summary, we have employed polarization- and azimuth-dependent FS-SFG to optically investigate hot electrons across the MoS_2/Au interface and their relaxation within the vicinity of the K point of the MoS_2 monolayer under ambient conditions, free from the interference by excitons. Compared to bare Au, significant differences were observed in the dynamics for the MoS_2 monolayer on Au, including much larger bleaching as well as distinct relaxation processes. As observed in both the bare Au and the MoS_2/Au system,

the relaxation process occurs on nearly identical timescales (∼2 ps), indicating that the equilibrium was established in the combined electronic system, as successfully elucidated by the simple kinetic model. Additionally, a defect-mediated process was proposed to account for the slower dynamics of hot-electron relaxation extending to around 60 ps. The current study establishes a robust, all-optical methodology to quantify ultrafast charge transfer across heterointerfaces. Beyond TMDC/metal systems, it is readily extendable to molecules adsorbed on TMDCs and to TMDC heterostructures under ambient conditions, and it can guide the design of TMDC-based devices with faster charge transfer through optimized contacts. In addition, using circularly polarized pump and probe pulses can provide access to valley-specific dynamics.

Acknowledgments. This work was funded by the Deutsche Forschungsgemeinschaft (DFG, German Research Foundation) through Projects No. A06, No. B02, and No. C05 within the SFB 1242 "Non-Equilibrium Dynamics of Condensed Matter in the Time Domain" (Project No. 278162697), through Germany's Excellence Strategy (EXC 2033 - 390677874 - RESOLV) and IRTG 2803 "2D Mature" (Project No. 461605777). Additional support was provided by the European Research Council, i.e., ERC- CoG-2017 SOLWET (Project No. 772286) to R.K.C.

Data availability. The data that support the findings of this article are not publicly available. The data are available from the authors upon reasonable request.

[1] Q. H. Wang, K. Kalantar-Zadeh, A. Kis, J. N. Coleman, and M. S. Strano, Electronics and optoelectronics of two-dimensional transition metal dichalcogenides, Nat. Nanotechnol. **7**, 699 (2012).

[2] T. Mueller and E. Malic, Exciton physics and device application of two-dimensional transition metal dichalcogenide semiconductors, npj 2D Mater Appl **2**, 29 (2018).

[3] D. B. Sulas-Kern, E. M. Miller, and J. L. Blackburn, Photoinduced charge transfer in transition metal dichalcogenide heterojunctions–towards next generation energy technologies, Energy Environ. Sci. **13**, 2684 (2020).

[4] X. Guo, Q. Li, Y. Liu, T. Jin, Y. Chen, L. Guo, and T. Lian, Enhanced light-driven charge separation and H_2 generation efficiency in WSe_2 nanosheet–semiconductor nanocrystal heterostructures, ACS Appl. Mater. Interfaces **12**, 44769 (2020).

[5] D. K. Schroder, *Semiconductor Material and Device Characterization* (Wiley, Hoboken, NJ, 2006).

[6] W. Li, Y. Liang, D. Yu, L. Peng, K. P. Pernstich, T. Shen, A. R. Hight Walker, G. Cheng, C. A. Hacker, C. A. Richter, Q. Li, D. J. Gundlach, and X. Liang, Ultraviolet/ozone treatment to reduce metal-graphene contact resistance, Appl. Phys. Lett. **102**, 183110 (2013).

[7] M. Chhowalla, D. Jena, and H. Zhang, Two-dimensional semiconductors for transistors, Nat. Rev. Mater. **1**, 16052 (2016).

[8] Y. Wang, J. C. Kim, R. J. Wu, J. Martinez, X. Song, J. Yang, F. Zhao, A. Mkhoyan, H. Y. Jeong, and M. Chhowalla, Van der Waals contacts between three-dimensional metals and two-dimensional semiconductors, Nature (London) **568**, 70 (2019).

[9] P.-C. Shen, C. Su, Y. Lin, A.-S. Chou, C.-C. Cheng, J.-H. Park, M.-H. Chiu, A.-Y. Lu, H.-L. Tang, M. M. Tavakoli, G. Pitner, X. Ji, Z. Cai, N. Mao, J. Wang, V. Tung, J. Li, J. Bokor, A. Zettl, C.-I. Wu, T. Palacios, L.-J. Li, and J. Kong, Ultralow contact resistance between semimetal and monolayer semiconductors, Nature (London) **593**, 211 (2021).

[10] C. Xu, H. W. Yong, J. He, R. Long, A. R. Cadore, I. Paradisanos, A. K. Ott, G. Soavi, S. Tongay, G. Cerullo, A. C. Ferrari, O. V. Prezhdo, and Z.-H. Loh, Weak distance dependence of hot-electron-transfer rates at the interface between monolayer MoS_2 and gold, ACS Nano **15**, 819 (2021).

[11] R. T. Tung, The physics and chemistry of the Schottky barrier height, Appl. Phys. Rev. **1**, 011304 (2014).

[12] A. Pelella, O. Kharsah, A. Grillo, F. Urban, M. Passacantando, F. Giubileo, L. Iemmo, S. Sleziona, E. Pollmann, L. Madauß, M. Schleberger, and A. Di Bartolomeo, Electron irradiation of metal contacts in monolayer MoS_2 field-effect transistors, ACS Appl. Mater. Interfaces **12**, 40532 (2020).

[13] F. Ceballos, Q. Cui, M. Z. Bellus, and H. Zhao, Exciton formation in monolayer transition metal dichalcogenides, Nanoscale **8**, 11681 (2016).

[14] P. Steinleitner, P. Merkl, P. Nagler, J. Mornhinweg, C. Schüller, T. Korn, A. Chernikov, and R. Huber, Direct observation of ultrafast exciton formation in a monolayer of WSe_2, Nano Lett. **17**, 1455 (2017).

[15] G. Wang, A. Chernikov, M. M. Glazov, T. F. Heinz, X. Marie, T. Amand, and B. Urbaszek, *Colloquium*: Excitons in atomically thin transition metal dichalcogenides, Rev. Mod. Phys. **90**, 021001 (2018).

[16] J. Madéo, M. K. L. Man, C. Sahoo, M. Campbell, V. Pareek, E. L. Wong, A. Al-Mahboob, N. S. Chan, A. Karmakar, B. M. K. Mariserla, X. Li, T. F. Heinz, T. Cao, and K. M. Dani, Directly visualizing the momentum-forbidden dark excitons and their dynamics in atomically thin semiconductors, Science **370**, 1199 (2020).

[17] C. Trovatello, F. Katsch, N. J. Borys, M. Selig, K. Yao, R. Borrego-Varillas, F. Scotognella, I. Kriegel, A. Yan, A. Zettl, P. J. Schuck, A. Knorr, G. Cerullo, and S. D. Conte, The ultrafast onset of exciton formation in 2D semiconductors, Nat. Commun. **11**, 5277 (2020).

[18] S. Dong, M. Puppin, T. Pincelli, S. Beaulieu, D. Christiansen, H. Hübener, C. W. Nicholson, R. P. Xian, M. Dendzik, Y. Deng, Y. W. Windsor, M. Selig, E. Malic, A. Rubio, A. Knorr, M. Wolf, L. Rettig, and R. Ernstorfer, Direct measurement of key exciton properties: Energy, dynamics, and spatial distribution of the wave function, Nat. Sci. **1**, e10010 (2021).

[19] J. E. Zimmermann, M. Axt, F. Mooshammer, P. Nagler, C. Schüller, T. Korn, U. Höfer, and G. Mette, Ultrafast charge-transfer dynamics in twisted MoS_2/WSe_2 heterostructures, ACS Nano **15**, 14725 (2021).

[20] R. Wallauer, R. Perea-Causin, L. Münster, S. Zajusch, S. Brem, J. Güdde, K. Tanimura, K.-Q. Lin, R. Huber, E. Malic, and U. Höfer, Momentum-resolved observation of exciton formation dynamics in monolayer WS_2, Nano Lett. **21**, 5867 (2021).

[21] A. Singh, G. Moody, K. Tran, M. E. Scott, V. Overbeck, G. Berghäuser, J. Schaibley, E. J. Seifert, D. Pleskot, N. M. Gabor, J. Yan, D. G. Mandrus, M. Richter, E. Malic, X. Xu, and X. Li, Trion formation dynamics in monolayer transition metal dichalcogenides, Phys. Rev. B **93**, 041401(R) (2016).

[22] Y. Yu, Z. Ji, S. Zu, B. Du, Y. Kang, Z. Li, Z. Zhou, K. Shi, and Z. Fang, Ultrafast plasmonic hot electron transfer in Au nanoantenna/MoS_2 heterostructures, Adv. Funct. Mater. **26**, 6394 (2016).

[23] X. Wen, S. Chen, J. Zhao, W. Du, and W. Zhao, Enhanced plasmonic hot-carrier transfer in Au/WS_2 heterojunctions under nonequilibrium condition, ACS Photonics **9**, 1522 (2022).

[24] T. Pincelli, T. Vasileiadis, S. Dong, S. Beaulieu, M. Dendzik, D. Zahn, S.-E. Lee, H. Seiler, Y. Qi, R. P. Xian, J. Maklar, E. Coy, N. S. Mueller, Y. Okamura, S. Reich, M. Wolf, L. Rettig, and R. Ernstorfer, Observation of multi-directional energy transfer in a hybrid plasmonic–excitonic nanostructure, Adv. Mater. **35**, 2209100 (2023).

[25] A. G. Čabo, J. A. Miwa, S. S. Grønborg, J. M. Riley, J. C. Johannsen, C. Cacho, O. Alexander, R. T. Chapman, E. Springate, M. Grioni, J. V. Lauritsen, P. D. C. King, P. Hofmann, and S. Ulstrup, Observation of ultrafast free carrier dynamics in single layer MoS_2, Nano Lett. **15**, 5883 (2015).

[26] F. Liu, Time- and angle-resolved photoemission spectroscopy (TR-ARPES) of TMDC monolayers and bilayers, Chem. Sci. **14**, 736 (2023).

[27] K. F. Mak and J. Shan, Photonics and optoelectronics of 2D semiconductor transition metal dichalcogenides, Nat. Photon. **10**, 216 (2016).

[28] D. Xiao, G.-B. Liu, W. Feng, X. Xu, and W. Yao, Coupled spin and valley physics in monolayers of MoS_2 and other Group-VI dichalcogenides, Phys. Rev. Lett. **108**, 196802 (2012).

[29] T. Handa, M. Holbrook, N. Olsen, L. N. Holtzman, L. Huber, H. I. Wang, M. Bonn, K. Barmak, J. C. Hone, A. N. Pasupathy, and X. Zhu, Spontaneous exciton dissociation in transition metal dichalcogenide monolayers, Sci. Adv. **10**, eadj4060 (2024).

[30] T. Yang, E. Pollmann, S. Sleziona, E. Hasselbrink, P. Kratzer, M. Schleberger, R. K. Campen, and Y. Tong, Interaction between a gold substrate and monolayer MoS_2: An azimuthal-dependent sum frequency generation study, Phys. Rev. B **107**, 155433 (2023).

[31] T. Yang, S. Sleziona, E. Pollmann, E. Hasselbrink, P. Kratzer, M. Schleberger, R. K. Campen, and Y. Tong, Isolating the optical response of a MoS_2 monolayer under extreme screening of a metal substrate, Phys. Rev. B **109**, L161402 (2024).

[32] C. Hong, H. Kim, Y. Tao, J. H. Lim, J. Y. Lee, and J.-H. Kim, Ultrafast hot carrier extraction and diffusion at the MoS_2/Au van der Waals electrode interface, Sci. Adv. **11**, eadr1534 (2025).

[33] See Supplemental Material at http://link.aps.org/supplemental/10.1103/t3fz-gqf9 for experimental and theoretical information, which includes details about sample preparation and characterization, laser setup, data analysis, and determination of the σ of the Gaussian function for fitting. Furthermore, a simple kinetic model was applied to understand the charge transfer between Au and MoS_2, which also contains Ref. [53].

[34] N. Kumar, S. Najmaei, Q. Cui, F. Ceballos, P. M. Ajayan, J. Lou, and H. Zhao, Second harmonic microscopy of monolayer MoS_2, Phys. Rev. B **87**, 161403(R) (2013).

[35] Y. Li, Y. Rao, K. F. Mak, Y. You, S. Wang, C. R. Dean, and T. F. Heinz, Probing symmetry properties of few-layer MoS_2 and h-BN by optical second-harmonic generation, Nano Lett. **13**, 3329 (2013).

[36] L. M. Malard, T. V. Alencar, A. P. M. Barboza, K. F. Mak, and A. M. de Paula, Observation of intense second harmonic generation from MoS_2 atomic crystals, Phys. Rev. B **87**, 201401(R) (2013).

[37] Z. Wang, C. Hong, Z. Sun, S. Wu, B. Liang, X. Duan, W.-T. Liu, and S. Wu, Contrast-enhanced phase-resolved second harmonic generation microscopy, Opt. Lett. **49**, 2117 (2024).

[38] W. S. Fann, R. Storz, H. W. K. Tom, and J. Bokor, Electron thermalization in gold, Phys. Rev. B **46**, 13592 (1992).

[39] J. Hohlfeld, S. S. Wellershoff, J. Güdde, U. Conrad, V. Jähnke, and E. Matthias, Electron and lattice dynamics following optical excitation of metals, Chem. Phys. **251**, 237 (2000).

[40] M. Bauer, A. Marienfeld, and M. Aeschlimann, Hot electron lifetimes in metals probed by time-resolved two-photon photoemission, Prog. Surf. Sci. **90**, 319 (2015).

[41] B. Liu, W. Zhao, Z. Ding, I. Verzhbitskiy, L. Li, J. Lu, J. Chen, G. Eda, and K. P. Loh, Engineering bandgaps of monolayer MoS_2 and WS_2 on fluoropolymer substrates by electrostatically tuned many-body effects, Adv. Mater. **28**, 6457 (2016).

[42] P. Majchrzak, K. Volckaert, A. G. Čabo, D. Biswas, M. Bianchi, S. K. Mahatha, M. Dendzik, F. Andreatta, S. S. Grønborg, I. Marković, J. M. Riley, J. C. Johannsen, D. Lizzit, L. Bignardi, S. Lizzit, C. Cacho, O. Alexander, D. Matselyukh, A. S. Wyatt, R. T. Chapman, E. Springate, J. V. Lauritsen, P. D. C. King, C. E. Sanders, J. A. Miwa, P. Hofmann, and S. Ulstrup, Spectroscopic view of ultrafast charge carrier dynamics in single- and bilayer transition metal dichalcogenide semiconductors, J. Electron Spectrosc. Relat. Phenom. **250**, 147093 (2021).

[43] V. Smejkal, F. Libisch, A. Molina-Sanchez, C. Trovatello, L. Wirtz, and A. Marini, Time-dependent screening explains the ultrafast excitonic signal rise in 2D semiconductors, ACS Nano **15**, 1179 (2021).

[44] J. Kang, W. Liu, D. Sarkar, D. Jena, and K. Banerjee, Computational study of metal contacts to monolayer transition-metal dichalcogenide semiconductors, Phys. Rev. X **4**, 031005 (2014).

[45] H. Lee, S. Deshmukh, J. Wen, V. Z. Costa, J. S. Schuder, M. Sanchez, A. S. Ichimura, E. Pop, B. Wang, and A. K. M. Newaz, Layer-dependent interfacial transport and optoelectrical properties of MoS_2 on ultraflat metals, ACS Appl. Mater. Interfaces **11**, 31543 (2019).

[46] E. Pollmann, S. Sleziona, T. Foller, U. Hagemann, C. Gorynski, O. Petri, L. Madauß, L. Breuer, and M. Schleberger, Large-Area, Two-dimensional MoS_2 exfoliated on gold: Direct experimental access to the metal–semiconductor interface, ACS Omega **6**, 15929 (2021).

[47] S. I. Anisimov, B. L. Kapeliovich, and T. L. Perel'man, Electron emission from metal surfaces exposed to ultrashort laser pulses, Sov. Phys. JETP **39**, 375 (1974).

[48] H. Wang, C. Zhang, and F. Rana, Ultrafast dynamics of defect-assisted electron–hole recombination in monolayer MoS_2, Nano Lett. **15**, 339 (2015).

[49] H.-P. Komsa and A. V. Krasheninnikov, Native defects in bulk and monolayer MoS_2 from first principles, Phys. Rev. B **91**, 125304 (2015).

[50] B. Schuler, D. Y. Qiu, S. Refaely-Abramson, C. Kastl, C. T. Chen, S. Barja, R. J. Koch, D. F. Ogletree, S. Aloni, A. M. Schwartzberg, J. B. Neaton, S. G. Louie, and A. Weber-Bargioni, Large spin-orbit splitting of deep in-gap defect states of engineered sulfur vacancies in monolayer WS_2, Phys. Rev. Lett. **123**, 076801 (2019).

[51] R. Krause, S. Aeschlimann, M. Chávez-Cervantes, R. Perea-Causin, S. Brem, E. Malic, S. Forti, F. Fabbri, C. Coletti, and I. Gierz, Microscopic understanding of ultrafast charge transfer in van der Waals heterostructures, Phys. Rev. Lett. **127**, 276401 (2021).

[52] A. Bruix, J. A. Miwa, N. Hauptmann, D. Wegner, S. Ulstrup, S. S. Grønborg, C. E. Sanders, M. Dendzik, A. G. Čabo, M. Bianchi, J. V. Lauritsen, A. A. Khajetoorians, B. Hammer, and P. Hofmann, Single-layer MoS_2 on Au(111): Band gap renormalization and substrate interaction, Phys. Rev. B **93**, 165422 (2016).

[53] D. M. Newns, Self-consistent model of hydrogen chemisorption, Phys. Rev. **178**, 1123 (1969).